The EMBO Journal (2010) 29, 2342–2357 | © 2010 European Molecular Biology Organization | All Rights Reserved 0261-4189/10
www.embojournal.org

THE EMBO JOURNAL

The human core exosome interacts with differentially localized processive RNases: hDIS3 and hDIS3L

Rafal Tomecki[1,2], Maiken S Kristiansen[3,5], Søren Lykke-Andersen[3,5], Aleksander Chlebowski[2,5], Katja M Larsen[4], Roman J Szczesny[1,2], Karolina Drazkowska[1,2], Agnieszka Pastula[2,6], Jens S Andersen[4], Piotr P Stepien[1,2], Andrzej Dziembowski[1,2,*] and Torben Heick Jensen[3,*]

[1]Department of Biophysics, Institute of Biochemistry and Biophysics, Polish Academy of Sciences, Warsaw, Poland, [2]Department of Genetics and Biotechnology, Faculty of Biology, University of Warsaw, Warsaw, Poland, [3]Department of Molecular Biology, Centre for mRNP Biogenesis and Metabolism, Aarhus University, Aarhus C, Denmark and [4]Department of Biochemistry and Molecular Biology, University of Southern Denmark, Odense, Denmark

The eukaryotic RNA exosome is a ribonucleolytic complex involved in RNA processing and turnover. It consists of a nine-subunit catalytically inert core that serves a structural function and participates in substrate recognition. Best defined in *Saccharomyces cerevisiae*, enzymatic activity comes from the associated subunits Dis3p (Rrp44p) and Rrp6p. The former is a nuclear and cytoplasmic RNase II/R-like enzyme, which possesses both processive exo- and endonuclease activities, whereas the latter is a distributive RNase D-like nuclear exonuclease. Although the exosome core is highly conserved, identity and arrangements of its catalytic subunits in different vertebrates remain elusive. Here, we demonstrate the association of two different Dis3p homologs—hDIS3 and hDIS3L—with the human exosome core. Interestingly, these factors display markedly different intracellular localizations: hDIS3 is mainly nuclear, whereas hDIS3L is strictly cytoplasmic. This compartmental distribution reflects the substrate preferences of the complex *in vivo*. Both hDIS3 and hDIS3L are active exonucleases; however, only hDIS3 has retained endonucleolytic activity. Our data suggest that three different ribonucleases can serve as catalytic subunits for the exosome in human cells.

The EMBO Journal (2010) **29,** 2342–2357. doi:10.1038/emboj.2010.121; Published online 8 June 2010

*Corresponding authors. A Dziembowski, Department of Biophysics, Institute of Biochemistry and Biophysics, Polish Academy of Sciences, ul. Pawinskiego 5a, 02-106 Warsaw, Poland. Tel.: +48 22 5922033; Fax: +48 22 6584176; E-mail: andrzejd@ibb.waw.pl
or TH Jensen, Department of Molecular Biology, Centre for mRNP Biogenesis and Metabolism, Aarhus University, C. F. Møllers Allé, Building 1130, Aarhus C 8000, Denmark. Tel.: +45 60202705; Fax: +45 86196500; E-mail: thj@mb.au.dk
[5]These authors contributed equally to this work
[6]Present address: Department of Immunology, Jagiellonian University Medical College, ul. Czysta 18, 31-121 Cracow, Poland

Received: 22 December 2009; accepted: 18 May 2010; published online: 8 June 2010

Subject Categories: RNA
Keywords: human exosome; ribonuclease; RNA degradation; RNase II/R enzymes; RNB domain

Introduction

An important contributor to the regulation of gene expression in eukaryotic cells is the control of RNA decay rates, including the elimination of transcripts by RNA surveillance pathways (Houseley *et al*, 2006; Doma and Parker, 2007; Vanacova and Stefl, 2007; Lebreton and Seraphin, 2008; Schmid and Jensen, 2008b; Houseley and Tollervey, 2009). Moreover, the majority, if not all, of eukaryotic primary transcripts are subject to processing reactions, often involving both endo- and exonucleolytic cleavages to create mature molecules with diverse cellular functions.

Central to these reactions is the evolutionary conserved multisubunit RNA exosome complex, which is the only essential 3′→5′ exoribonuclease in *Saccharomyces cerevisiae*. It was first discovered for its function in 5.8S rRNA processing and later found to contribute to most cellular processes in eukaryotes involving RNA degradation from the 3′ end (Mitchell *et al*, 1997; Schmid and Jensen, 2008a). In the cytoplasm, the exosome participates in 3′→5′ decay of the mRNA body after its deadenylation (Anderson and Parker, 1998). It also has a function in the regulated degradation of transcripts containing AU-rich elements and of mRNAs cleaved by Argonaute proteins during RNA interference (RNAi) (Mukherjee *et al*, 2002; Gherzi *et al*, 2004; Orban and Izaurralde, 2005). In addition, the exosome helps to preclude the translation of defective mRNAs as it functions, together with other degradative activities, in the nonsense-mediated decay, nonstop decay and no-go decay pathways to remove RNA molecules with sequences that hinder proper ribosome translocation during translation (Doma and Parker, 2007; Isken and Maquat, 2007). Studies in yeast have revealed a nuclear function of the exosome in the maturation of rRNA, tRNA, snRNA and snoRNA, as well as in the degradation of RNA processing by-products. Moreover, mRNAs produced in yeast mutants with defective pre-mRNA processing or mRNP packaging are rapidly degraded by the exosome (Bousquet-Antonelli *et al*, 2000; Hilleren *et al*, 2001; Libri *et al*, 2002; Torchet *et al*, 2002; Rougemaille *et al*, 2007; Saguez *et al*, 2008). Finally, different classes of non-coding transcripts, including yeast cryptic unstable transcripts, antisense RNAs and human promoter-upstream transcripts (PROMPTs) also fall prey to the exosome (Wyers *et al*, 2005; Camblong *et al*, 2007; Houseley *et al*, 2008; Preker *et al*, 2008; Neil *et al*, 2009; Xu *et al*, 2009). How the exosome can target such a variety of substrates is still the subject of intense investigations, however, it is assumed that its specificity is, at least partly, achieved through the interaction

with accessory factors such as the nuclear complexes TRAMP and Nrd1p/Nab3p/Sen1p as well as the cytoplasmic Ski7p GTPase/SKI complex (Araki *et al*, 2001; LaCava *et al*, 2005; Orban and Izaurralde, 2005; Vasiljeva and Buratowski, 2006).

The eukaryotic exosome itself is an ~400 kDa multimeric complex, consisting of nine core subunits, six of which surround a central channel and contain domains homologous to the bacterial phosphorolytic ribonuclease RNase PH (Hernandez *et al*, 2006; Liu *et al*, 2006). The remaining three core subunits harbour S1 or KH RNA-binding domains and are positioned on top of the RNase PH-like ring. A highly similar architecture is found in RNA degrading complexes from other domains of life, such as the *Escherichia coli* polynucleotide phosphorylase (PNPase) and the archaeal exosome-like complexes (reviewed in Lorentzen *et al*, 2008a; Lykke-Andersen *et al*, 2009). However, despite the structural similarity, these complexes are phosphorolytic ribonucleases, whereas the yeast and human exosome cores are catalytically inactive (Liu *et al*, 2006; Dziembowski *et al*, 2007).

The yeast exosome is exclusively a hydrolase obtaining this catalytic activity from its 10th subunit Dis3p (Rrp44p), which resides both in the nucleus and in the cytoplasm (Mitchell *et al*, 1997; Allmang *et al*, 1999). Dis3p domain organization is similar to that of *E. coli* RNase II/R enzymes, except for the presence of a PilT N-terminal (PIN) domain at the N-terminus. The RNase II/R-homology region consists of three oligonucleotide-binding-fold RNA-binding domains (cold-shock domains 1 and 2 at the N-terminus and an S1 domain at the C-terminus) and a central RNase II catalytic (RNB) domain, responsible for the $3' \rightarrow 5'$ exonucleolytic activity (Frazao *et al*, 2006; Zuo *et al*, 2006). A single-point mutation within this domain (D551N) completely abolishes Dis3p exonuclease activity, both alone and in the presence of the exosome core (Dziembowski *et al*, 2007). It was recently demonstrated that Dis3p, through its PIN domain, is also endowed with an endonucleolytic activity (Lebreton *et al*, 2008; Schaeffer *et al*, 2009; Schneider *et al*, 2009), which strictly depends on conserved acidic residues (E120 and the D91–D171–D198 triad), predicted to coordinate a divalent cation in its catalytic centre. *In vivo* evidence indicates that cooperation between endo- and exonucleolytic activities of Dis3p is crucial for efficient degradation/processing of several natural exosome substrates (Lebreton *et al*, 2008; Schaeffer *et al*, 2009; Schneider *et al*, 2009). Perhaps endonucleolytic cleavages provide alternative entry sites for exonucleolytic degradation when exosome progression is blocked by RNA secondary structures. Importantly, apart from its endonucleolytic activity, the PIN domain also has a significant structural function by stably associating Dis3p with the exosome core through its direct contact with the Rrp41p subunit (Bonneau *et al*, 2009; Schneider *et al*, 2009).

In the yeast nucleus, the 10-subunit exosome associates with an additional catalytic subunit, Rrp6p. Contrary to the highly processive Dis3p enzyme, Rrp6p is a distributive exonuclease homologous to *E. coli* RNase D. Rrp6p is non-essential; however, *RRP6* deletion strains are temperature sensitive and many nuclear effects of core exosome mutation are recapitulated in *rrp6*Δ cells. Interestingly, the human Rrp6p ortholog hRRP6 (also called PM/SCl-100 or EXOSC10) is not nucleus-restricted but also reportedly present in the cytoplasm (Lejeune *et al*, 2003; van Dijk *et al*, 2007).

The nine-subunit human exosome core was, unlike its yeast counterpart, initially suggested to display phosphorolytic activity through the hRRP41 (EXOSC4) subunit (Liu *et al*, 2006). However, this turned out to be trace contamination of the reconstituted complex with *E. coli* PNPase. Thus, a fundamental question is which protein is the major catalytic subunit of the human exosome. As the nucleolytic activity of yeast Rrp6p is distributive, it is unlikely that hRRP6 is responsible for the bulk of human exosome activity. Instead, the most natural candidate would be the closest sequence homolog of yeast Dis3p, hDIS3 (also called hRRP44). Consistent with this notion, exogenously expressed *hDIS3* complements the severe growth phenotype of a temperature-sensitive mutation of the *S. cerevisiae DIS3* gene (Shiomi *et al*, 1998). Still, the interaction of hDIS3 with the exosome core has been questioned, as hDIS3 was absent from preparations of the endogenous complex (Chen *et al*, 2001). Further studies of the human exosome have focused on its catalytically inactive subunits hRRP45 (PM/SCl-75/EXOSC9), hRRP41 (EXOSC4) or hRRP4 (EXOSC2) as well as hRRP6 and cofactors of the nuclear exosome: C1D, hMTR4 (SKIV2L2) and hMPP6 (Schilders *et al*, 2005, 2007; West *et al*, 2006; van Dijk *et al*, 2007; Mullen and Marzluff, 2008). Although these factors are found to be required for the maintenance of human exosome integrity and efficient degradation and/or processing of various RNA classes, the central question of what constitutes the major catalytic activity has been left unanswered.

In this paper, we reveal by proteomic analyses that two human orthologs of yeast Dis3p, hDIS3 and hDIS3L, both interact with the exosome core. Subcellular localization analyses and *in vivo* examination of substrate specificities demonstrate that while hDIS3L is entirely cytoplasmic, hDIS3 is predominantly nuclear. Interestingly, hDIS3 is excluded from the nucleolus, where instead hRRP6 accumulates. *In vitro* assays demonstrate that both hDIS3 and hDIS3L display processive exonuclease activity; however, only hDIS3 is an active endonuclease. Finally, only hDIS3 is able to partially complement lowered levels of yeast Dis3p, an ability that strictly depends on an intact RNB domain. Thus, exosomal organization of ribonucleolytic activities differs markedly between yeast and human cells.

Results

The human genome encodes two PIN domain-containing homologs of yeast Dis3p

Until the first draft of the human genome, only one ortholog of *S. cerevisiae* Dis3p had been identified (Shiomi *et al*, 1998). However, with the human genome sequence in hand, three genes with similarities to yeast *DIS3* are apparent. For two of these, the predicted protein products have the same domain architecture as yeast Dis3p—an RNase II/R homologous region with an RNB domain, and an N-terminal PIN domain (Figure 1A). We hereafter refer to these proteins as hDIS3 and hDIS3-like (hDIS3L), as the homology is stronger between Dis3p and hDIS3 (43% identity) than between Dis3p and hDIS3L (33%) (see Supplementary Figure S1A for a full-sequence alignment of Dis3p with its human and mouse orthologs). This situation is observed in all completely sequenced vertebrate genomes (Supplementary Figure S1B), pointing to at least one gene duplication of *DIS3* during the

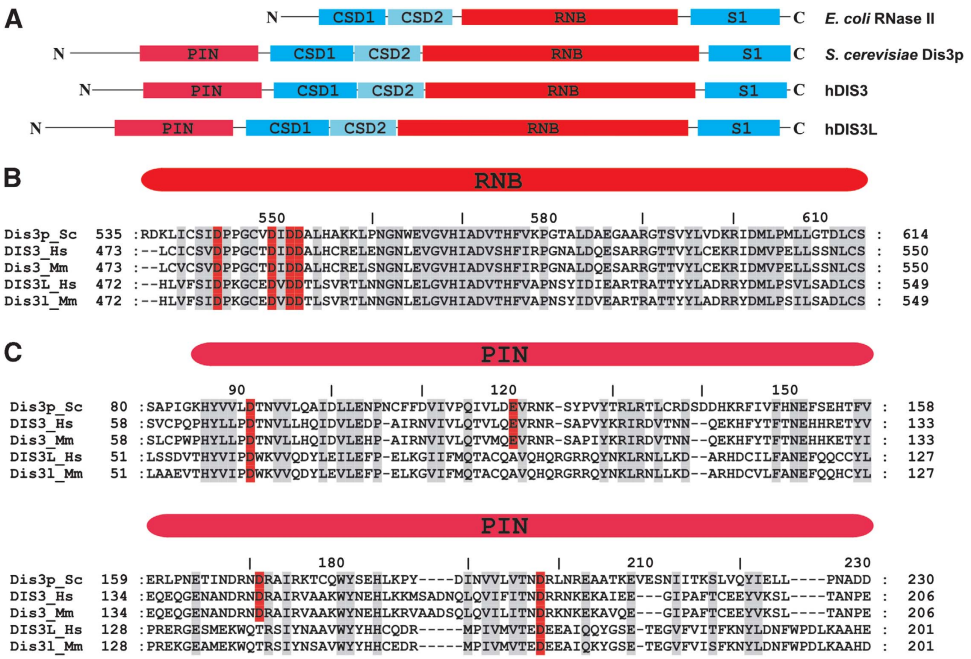

Figure 1 Mammalian genomes encode two proteins, Dis3 and Dis3L, with domain composition identical to that of yeast Dis3p. (**A**) Domain organization of RNase II/R enzymes from different species. *E. coli* RNase II and Dis3 proteins from yeast and humans contain an RNase II/R-like region featuring a similar modular arrangement with two cold-shock domains (CSD1 and CSD2), an RNB domain and a C-terminal S1 domain. In addition, Dis3 factors have an extended N-terminal part including the PIN domain. (**B**) Sequence alignment of the RNB domains of *S. cerevisiae* Dis3p (Dis3p_Sc), *Homo sapiens* hDIS3 (accession BAF92610) and hDIS3L (accession Q8TF46) (DIS3_Hs and DIS3L_Hs) and *Mus musculus* Dis3 and Dis3L (Dis3_Mm and Dis3l_Mm). The four conserved aspartic acid residues marked in red are involved in the coordination of magnesium in the catalytic centre. (**C**) Sequence alignment of the PIN domains of the five Dis3 proteins from (**B**). The four acidic residues essential for catalysis are marked in red. Two of these are absent from the Dis3L proteins.

course of evolution. The third Dis3p-like protein, referred to as hDIS3-like 2 (hDIS3L2), also contains the RNase II/R homology region but lacks the PIN domain responsible for association with the exosome core. We thus predicted that hDIS3L2 is unable to cooperate with the exosome and did not study it further.

Several amino-acid residues within the RNB domain of Dis3p are inferred to be involved in catalysis and substrate binding (Lorentzen *et al*, 2008b). Most of these are conserved in both hDIS3 and hDIS3L, in particular the four aspartic acid residues responsible for magnesium ion coordination, including the one corresponding to the Dis3p D551 position, which is critical for exonucleolytic activity (Dziembowski *et al*, 2007) (Figure 1B). However, in the case of the PIN domain, only hDIS3 contains all conserved amino acids essential for endonucleolytic activity. In hDIS3L, two of the acidic residues important for this activity (corresponding to E120 and D171 in yeast Dis3p) are replaced by alanine (position 90) and threonine (position 140), respectively (Figure 1C). In murine homologs, the amino-acid conservation of the RNB and PIN domains is virtually identical to the human DIS3 variants (Figure 1B and C).

To assess whether the human homologues of Dis3p can functionally replace the yeast protein, we performed complementation assays in the context of Dis3p depletion. As this factor is essential, we used a yeast strain with endogenous *DIS3* under the control of a tetracycline-repressible promoter. Its downregulation by the addition of doxycycline depletes Dis3p and severely inhibits growth, which can be fully restored by exogenous expression of Dis3p (Lebreton *et al*, 2008; Figure 2A, upper part). We observed partial complementation of Dis3p depletion by expression of hDIS3, whereas hDIS3L did not sustain growth in this context (Figure 2A, upper part). Northern blotting analysis revealed that both human ORFs are actively transcribed in yeast (Figure 2B). However, as we could not detect the respective proteins using antibodies against hDIS3 and hDIS3L (data not shown), we repeated the complementation experiment using C-terminally FLAG-tagged hDIS3 and hDIS3L constructs, which yielded an essentially identical result as for the constructs encoding untagged proteins (Figure 2A, bottom part). Transcripts corresponding to hDIS3-FLAG and hDIS3L-FLAG were detected by northern analysis (Figure 2B). Moreover, affinity purification of native protein extracts on anti-FLAG beads concentrated the hDIS3-FLAG and hDIS3L-FLAG proteins sufficiently to allow their detection by Coomassie staining (Figure 2C, upper part), western blotting (Figure 2C, bottom part) and mass spectrometry (MS) (data not shown).

Taken together, the exclusive ability of hDIS3 to partially complement yeast Dis3p depletion suggests that some functional differences between hDIS3 and hDIS3L exist.

hDIS3 and hDIS3L both coimmunoprecipitate with the human core exosome

Given the strong conservation between eukaryotic exosomes, hDIS3 and hDIS3L would be expected to associate with the exosome core. Nonetheless, an earlier purification of the human exosome did not coprecipitate these proteins (Chen *et al*, 2001). To revisit this question, we used stable isotope labelling with amino acids in cell culture (SILAC) followed by MS analysis. Because of the selective amino-acid labelling of

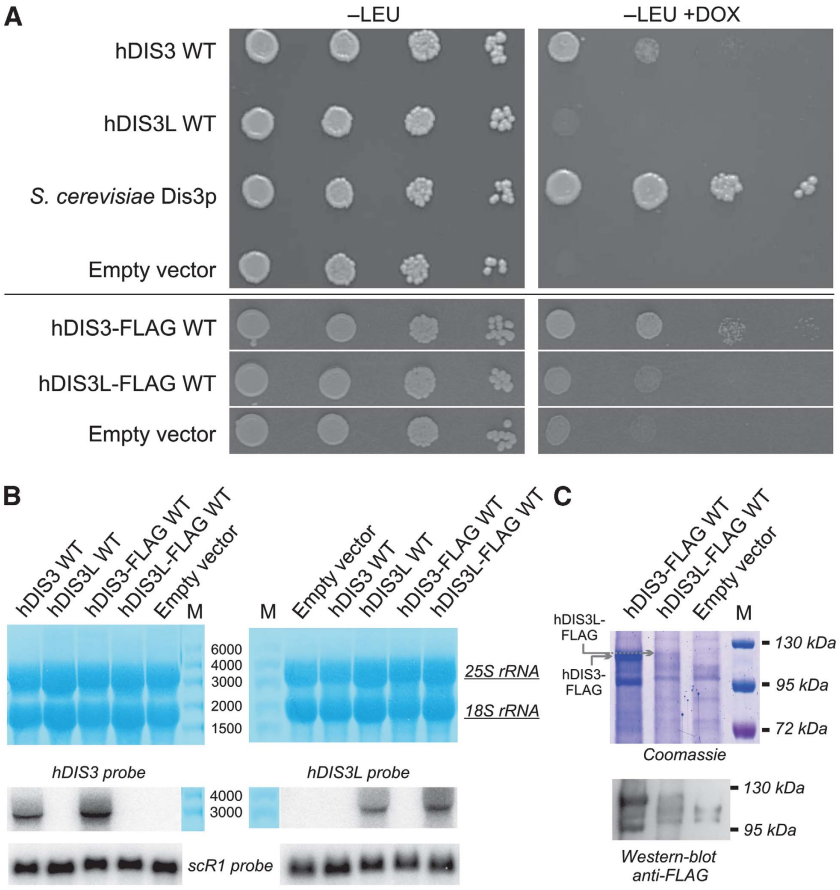

Figure 2 hDIS3, but not hDIS3L, complements a Dis3p-depleted yeast strain. (**A**) Yeast complementation assay. LEU-marked plasmids containing *hDIS3*, *hDIS3L*, yeast *DIS3* or no insert (empty vector control) were transformed into a strain harbouring endogenous *DIS3* under control of a doxycycline-repressible promoter. Growth phenotypes of the resulting strains were analysed after 60 h in the absence (−LEU, endogenous *DIS3* expressed) or presence (−LEU +DOX, endogenous *DIS3* repressed) of doxycycline (upper part). Analogous analysis was done using plasmids encoding hDIS3-FLAG and hDIS3L-FLAG fusions (bottom part). (**B**) Northern blotting analysis of hDIS3 and hDIS3L transcripts from selected total RNA samples from (**A**). Methylene-blue staining of the membrane after transfer (top) and re-hybridization of the blot with a scR1 probe (bottom) served as loading controls. M—RiboRuler High Range RNA Ladder (Fermentas) with bands' sizes (in nucleotides) indicated. (**C**) hDIS3 and hDIS3L protein production from the expression plasmids used in (**A**). Anti-FLAG beads with bound proteins purified from extracts from yeast transformed with constructs coding for either hDIS3-FLAG or hDIS3L-FLAG, or an empty vector were subjected to SDS–PAGE analysis (top) or western blotting using anti-FLAG antibodies (bottom). M—PageRuler Prestained Protein Ladder (Fermentas) with molecular masses indicated.

test and control samples, this methodology allows the reliable discrimination between specific interactors and background contaminants even when the assumed binding affinity is weak (Ong *et al*, 2003). We therefore established stable HEK293 Flp-In T-REx cell lines, which can be induced by tetracycline to express C-terminally FLAG-tagged versions of hRRP41, hDIS3L and hDIS3. Control cells supplemented with one amino-acid isotope mix were left uninduced, whereas expression of the relevant bait protein was induced in test cells supplemented with another amino-acid isotope mix. After loading of the two cell extracts onto separate anti-FLAG antibody columns, which were extensively washed, columns were mixed and eluted with either excess FLAG peptide (hRRP41 experiment) or SDS (hDIS3 and hDIS3L experiments). Eluates were checked for the presence of the bait protein by western blotting (Figure 3A) and subjected to MS analysis.

The hRRP41-FLAG bait coprecipitates the entire exosome core as well as exosome cofactors hRRP6, hMTR4 and hMPP6, with SILAC ratios clearly above background (Figure 3B, left column). The presence of all these components is revealed by multiple peptides in the sample (Supplementary Table S1). Interestingly, hDIS3L also emerges as a specific hRRP41 binder. Although in this experiment, the interaction is evident by only one manually validated peptide in the MS spectrum, it appears highly specific as the hDIS3L-FLAG bait in turn coprecipitates the entire core exosome as well as hRRP6 and hMTR4 with robust SILAC ratios (Figure 3B, right column; Supplementary Table S3).

Initial purification attempts using the hDIS3-FLAG bait yielded only a few peptides arising from exosome components (data not shown). We therefore performed the experiment under less stringent conditions lowering the NaCl concentration in the binding and washing solutions from 100 to 75 mM. This change in experimental protocol resulted in the purification of 7 out of 9 core components in addition to hRRP6 and hMTR4 (Figure 3B, middle column; Supplementary Table S2). Although some peptide counts are sparse, SILAC ratios verified the specificity of the interactions.

hDIS3 and hDIS3L interaction with components of the exosome core was confirmed by IgG affinity purifications

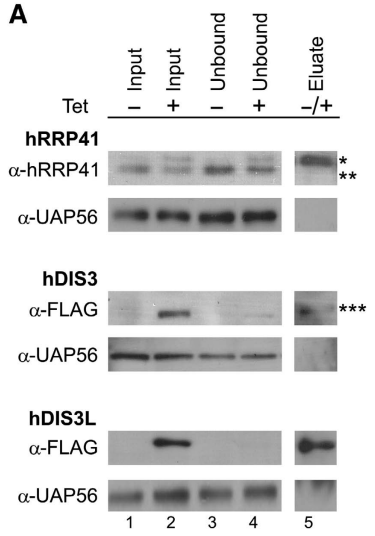

B

hRRP41-CoIP (100 mM NaCl)		hDIS3-CoIP (75 mM NaCl)		hDIS3L-CoIP (100 mM NaCl)			
Protein	*SILAC ratio*	*Protein*	*SILAC ratio*	*Protein*	*SILAC ratio*	*Protein*	*SILAC ratio*
hRRP42	>10	**hDIS3**	>10	GIGYF2	>10	**hMTR4**	4.8
hCSL4	>10	**hRRP45**	5.8	ZNF598	>10	HBS1L	2.3
hRRP41	>10	**hRRP46**	5.6	**hDIS3L**	9.0	HSPA1A	1.7
hRRP4	>10	**hCSL4**	5.4	eIF4E2	7.3	**hRRP4**	1.7
hRRP45	>10	**hRRP4**	5.2	**hRRP41***	7.0		
hMPP6	>10	**hRRP41***	5.2	**hRRP46**	6.8		
hRRP40	>10	**hRRP6**	4.7	**hRRP6**	6.7		
hMTR4	>10	**hRRP42**	4.6	**hRRP45**	6.7		
hRRP46	>10	**hRRP43**	3.0	**hRRP42**	6.3		
hRRP6	>10	**hMTR4**	2.9	**hRRP4**	6.0		
hMTR3	>10			**hRRP40**	5.9		
hDIS3L*	9.7			**hMTR3***	5.7		
hRRP43	7.8			**hCSL4**	5.3		
				hRRP43	5.0		

Figure 3 hDIS3 and hDIS3L can copurify the human exosome core. (**A**) Western blotting analyses of hRRP41-FLAG (top), hDIS3-FLAG (middle) and hDIS3L-FLAG (bottom) anti-FLAG precipitations. Uninduced (−) or tetracycline-induced (+) cells were grown in SILAC media. Input and unbound fractions, as well as eluates, were probed with α-RRP41 or α-FLAG antibodies as indicated. α-UAP56 antibodies were used as a control. *, ** and *** indicate hRRP41-FLAG, endogenous hRRP41 and hDIS3-FLAG, respectively. (**B**) hRRP41, hDIS3 and hDIS3L copurifying proteins identified by MS. Exosome core components and accessory factors are shown in bold. Only proteins with a SILAC ratio above background (see Materials and methods) are shown. Moreover, proteins detected by only one peptide are omitted unless they are known exosome components, in which case the MS spectra was manually validated and the protein was marked with an asterisk. In the interest of space, the list of interactors is cut after the last identified exosome component. For full data sets, including protein scores, see Supplementary Tables S1–S3).

using stable HEK293 Flp-In T-REx cell lines producing C-terminally TAP-tagged hDIS3 or hDIS3L (Supplementary Figure S2). Taken together, our data demonstrate that both *S. cerevisiae* Dis3p homologs—hDIS3 and hDIS3L—are capable of interacting with the human core exosome, albeit with seemingly lower affinities than their *S. cerevisiae* counterpart.

Different subcellular localizations of hDIS3 and hDIS3L

We next wanted to determine the subcellular localizations of hDIS3 and hDIS3L. In addition, we revisited the localization of hRRP6 as earlier reports surprisingly found that, in contrast to yeast Rrp6p, a small pool of this protein resides in the cytoplasm (Lejeune *et al*, 2003; van Dijk *et al*, 2007). To avoid artefacts, we used several different reagents and localized the proteins in both HEK293 Flp-In T-REx and HeLa cells. First, we used commercially available anti-hDIS3 antibodies to stain HeLa cells. Confocal microscopy revealed that hDIS3 localizes mainly to the nucleus, where it appears to be excluded from areas interpreted to be nucleoli by virtue of their morphology and absence of DNA staining by Hoechst 33342 (Figure 4A). Moreover, with this reagent a weak punctuate cytoplasmic hDIS3 staining pattern, the significance of which is presently unclear, can also be observed. This localization of hDIS3 was largely confirmed by epifluorescent microscopy using the same antibody to stain HEK293 Flp-In T-REx cells (Figure 4E), whereas confocal microscopy using anti-FLAG antibody to visualize the hDIS3-FLAG protein from the stable cell line used for the proteomic studies only yielded a nuclear signal (Supplementary Figure S3). Thus, with these assays, the majority of hDIS3 appears nuclear with a possible minor cytoplasmic pool.

To localize hDIS3L, we initially introduced a C-terminal c-myc fusion of hDIS3L into HEK293 Flp-In T-REx cells. Anti-myc immunostaining followed by confocal microscopy revealed this fusion protein to be exclusively cytoplasmic (Figure 4B). This result was reproduced by both epifluorescent microscopic analysis of HEK293 Flp-In T-REx cells stained with either an antibody recognizing endogenous hDIS3L (Figure 4E) or anti-FLAG staining of the hDIS3L-FLAG-expressing HEK293 Flp-In T-REx cells (Supplementary Figure S3). In the former case, specificity was ascertained by the disappearance of the hDIS3L signal on depletion of the protein by RNAi (data not shown). In addition, localization studies in HeLa cells of a C-terminally tagged EGFP fusion of hDIS3L yielded a similar result (data not shown). We conclude that despite their sequence homology and their common association with the core exosome, hDIS3 and hDIS3L distribute differently in the cell.

Finally, a commercial anti-hRRP6 antibody showed that this factor localizes primarily to the nucleus of HeLa cells (Figure 4C). However, in contrast to hDIS3, hRRP6 is strongly enriched in nucleoli. This result was confirmed using hRRP6-FLAG and EGFP-tagged proteins as well as the commercial anti-hRRP6 antibody on HEK293 Flp-In T-REx cells (Figure 4E; Supplementary Figure S3 and data not shown). Importantly, a weak, but consistent, cytoplasmic signal is also revealed by the anti-hRRP6 and anti-FLAG antibodies (Figure 4C and E; Supplementary Figure S3) and the EGFP fusion (data not shown).

The differential localization of hDIS3, hDIS3L and hRRP6 was unexpected. We therefore tested this result by an independent procedure of subcellular fractionation of cells followed by western blotting analysis of the different fractions. The validity of this protocol was verified by the expected localization of tubulin, U1 70K and histone H3 to the cytoplasmic, nuclear and chromatin fractions, respectively (Figure 4D). Using this technique, it was evident that

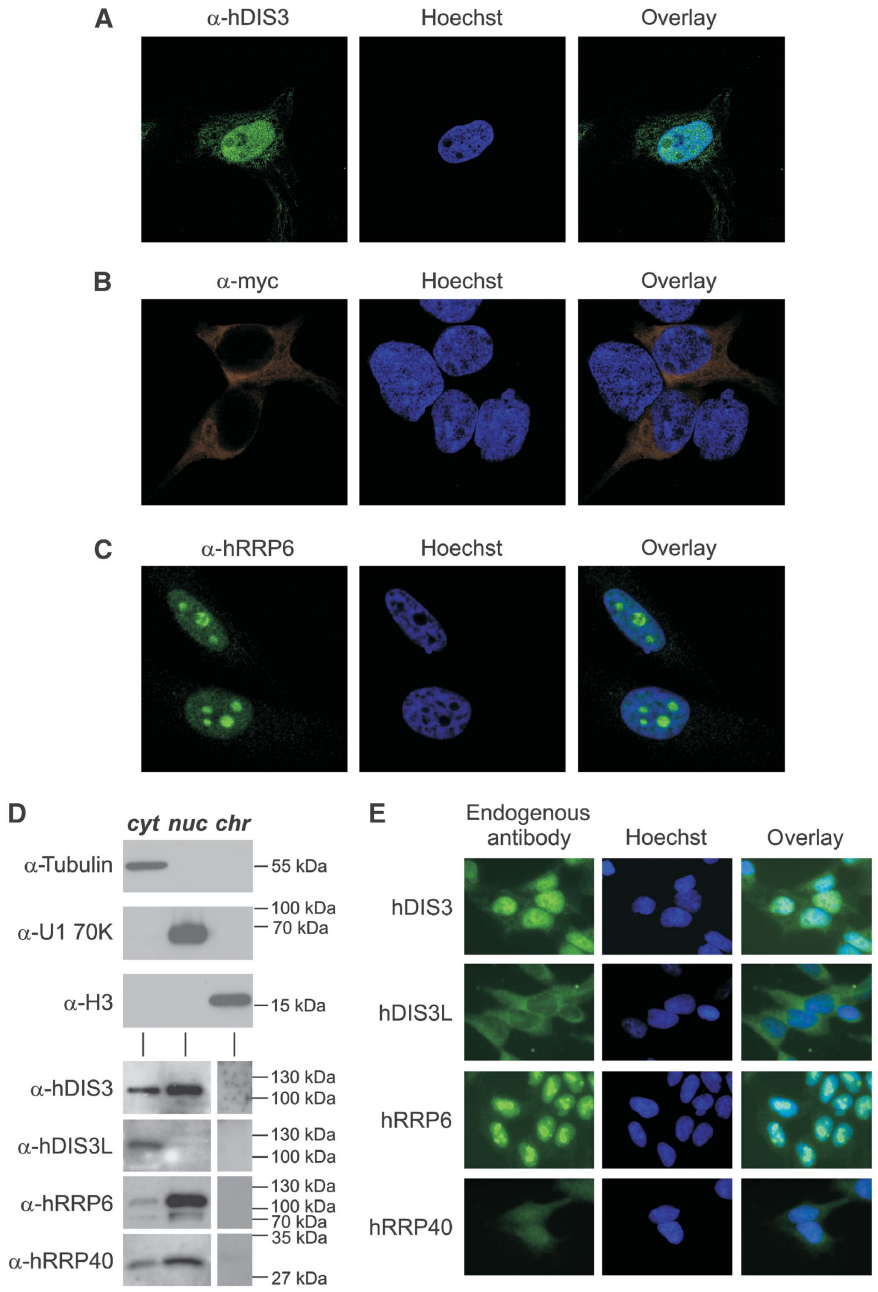

Figure 4 Differential subcellular localization of the three human exosome complex catalytic subunits. (**A**) Endogenous hDIS3 is localized mainly in the nucleus with a smaller amount in the cytoplasm. HeLa cells were subjected to immunofluorescence analysis using anti-hDIS3 antibody and visualized by confocal microscopy. Nuclei were stained with Hoechst dye. (**B**) An hDIS3L-myc fusion protein localizes exclusively to the cytoplasm. HEK293 Flp-In T-REx cells were transiently transfected with a plasmid bearing hDIS3L-c-myc. Protein expression was induced for 12 h with doxycycline and 24 h after transfection cells were subjected to immunofluorescence staining and confocal microscopy. (**C**) Endogenous hRRP6 is mainly nuclear with enrichment in the nucleoli, and some cytoplasmic staining. HeLa cells were subjected to immunofluorescence using anti-hRRP6 antibodies and inspected by confocal microscopy. (**D**) Analysis of the distribution of different exosome subunits in subcellular fractions of HEK293 Flp-In T-REx cells. Nuclei, cytoplasm and chromatin were separated by fractionation and similar cell equivalents were subjected to SDS–PAGE followed by western blotting using the indicated antibodies. hDIS3, hRRP6 and hRRP40 display varying degrees of dual nucleo-cytoplasmic localization, whereas hDIS3L is localized exclusively in the cytoplasm. Tubulin, the U1 70K splicing factor and histone H3 serve as cytoplasmic, nuclear and chromatin markers, respectively. The nuc/cyt fractions and the chromatin fractions were run on different gels. (**E**) Verification of the cellular fractionation analysis of (**D**) by HEK293 Flp-In T-REx cell staining of endogenous hDIS3, hDIS3L, hRRP6 and hRRP40 as indicated. Cells were inspected by epifluorescence microscopy.

hDIS3L is restricted to the cytoplasm. Nuclear and cytoplasmic fractions both contain hDIS3, the exact partitioning of which is subject to slight experimental variation. Moreover, a small, but reproducible, amount of hRRP6 is detected in the cytoplasmic fraction (Figure 4D). As expected, an exosome core subunit, hRRP40, is present in both nuclear and cytoplasmic fractions, which was verified by immunolocalization analysis (Figure 4E). In sum, two different approaches largely reach the same conclusion: whereas hDIS3L is exclusively cytoplasmic, hDIS3 and hRRP6 are mostly nuclear proteins.

However, their intranuclear distribution is different as hDIS3 is excluded from nucleoli, whereas hRRP6 is more abundantly localized to this nuclear body.

In vivo impact of three human exosome-associated nucleases

To conduct a preliminary examination of the differential localizations of hDIS3, hDIS3L and hRRP6 on exosome activity *in vivo*, we took advantage of the HEK293 Flp-In T-REx cell lines expressing hDIS3-FLAG, hDIS3L-FLAG and hRRP6-FLAG to make a rough estimation of their relative endogenous stoichiometries. As a common measure for core exosome levels, the cell line expressing hRRP40-FLAG was also included. First, western blotting analyses using antibodies towards the different endogenous proteins were performed to determine their levels of overexpression on induction with tetracycline (Supplementary Figure S4A, upper panel). A second round of westerns using anti-FLAG antibodies on the same tetracycline-induced samples established cellular levels of the three overexpressed proteins relative to each other (Supplementary Figure S4A, lower panel). Using these numbers, we estimate that while hDIS3 and hDIS3L are present in HEK293 cells in an approximate 1:1 ratio, hRRP6 and hRRP40 are in ~10-fold molar excess (Supplementary Figure S4B). Although, these analyses are only semi-quantitative and should be interpreted with caution, the molar excess of hRRP6 to hDIS3 and hDIS3L may explain why a distributive exonuclease importantly impacts the function of the core exosome, which is also capable of associating with processive enzymes.

To further elaborate on the significance of the differential localization of hDIS3, hDIS3L and hRRP6, we tested the effect of their depletion by RNAi on the cellular levels and processing patterns of three sets of substrates in HeLa cells; the presumed nuclear-degraded PROMPTs (Preker *et al*, 2008), the nuclear processed 5.8S rRNA as well as the *c-MYC* and *c-FOS* mRNAs, the majority of which are degraded in the cytoplasm. Western blotting analysis revealed that the three nucleases could be depleted efficiently both by knocking down individual proteins as well as all their possible combinations (Figure 5A). Interestingly, hRRP6 depletion leads to the upregulation of hDIS3L and conversely hDIS3 and hDIS3L depletions result in slightly elevated levels of hRRP6. This argues that these enzymes have some redundant function(s) and that the cell is trying to compensate the loss of one by increasing levels of another. Perhaps an ability to compensate, also with other degradation machineries, is part of the explanation why none of the knockdown combinations had a particularly strong impact on cell growth (Supplementary Figure S5), at least over the time span measured. This observation is in contrast to the situation reported for HepG2 cells (van Dijk *et al*, 2007), and may therefore reflect an ability of HeLa cells to tolerate lower levels of exosome activity. Finally, as observed earlier, knockdown of hRRP40 also depletes hRRP6 (Kammler *et al*, 2008), a phenomenon which is also evident for hDIS3L (Figure 5A).

Total RNA harvested from the siRNA-treated cells was subjected to reverse transcription (RT) using an oligo(dT) primer followed by quantitative PCR (qPCR) using primers specific for four PROMPT regions. As described earlier (Preker *et al*, 2008), all four substrates are robustly stabilized on double depletion of hRRP6 and hDIS3 compared with the control; single knockdowns of these enzymes yield much lower effects (Figure 5C). As also seen earlier, depletion of hRRP40 leads to a comparable degree of stabilization. As hDIS3 levels are normal in the hRRP40 knockdown, this suggests that hDIS3 requires an intact exosome core for function. Interestingly, depletion of hDIS3L does not contribute appreciably to the stabilization of PROMPTs in neither single, double nor triple knockdown constellations. A consistent set of observations was made when assaying 5.8S rRNA processing by northern blotting analysis. Again single hRRP6 and hDIS3 depletions resulted in the accumulation of 5.8S rRNA precursors, an effect that was exacerbated in the hRRP6/hDIS3 double knockdown (Figure 5B). However, neither as an individual knockdown nor in addition to the hRRP6-, hDIS3- or hRRP6/hDIS3-depletions did hDIS3L depletion have an effect. Both PROMPT and 5.8S rRNA results are therefore consistent with the idea that hDIS3L does not exert its effect in the nucleus.

A possible cytoplasmic function of hDIS3L was assessed by investigating steady-state levels of *c-MYC* and *c-FOS* mRNAs from the various samples. For *c-MYC* mRNA, the hRRP6/hDIS3 double knockdown yielded an ~2.5-fold stabilization, which increased to ~4-fold when adding the hDIS3L siRNAs (Figure 5D, left panel). This level of stabilization was also obtained on hRRP40 depletion. For *c-FOS* mRNA stabilization, the hRRP40 knockdown had the greatest impact, however, also here an effect of depleting hDIS3L can be observed; the ratio of *c-FOS* mRNA stabilization rises from ~2-fold in the hRRP6/hDIS3 double knockdown to ~4-fold when all three exonucleases are depleted (Figure 5D, right panel). These data again support the notion that hDIS3L serves a function in the cytoplasm, whereas hDIS3 mainly operates in the nucleus. This is also in agreement with recent publications reporting accumulation of polyadenylated RNA decay intermediates in the cytoplasm on hDIS3L depletion (Slomovic *et al*, 2010; Staals *et al*, 2010).

Both hDIS3 and hDIS3L are 3′→5′ exonucleases but only hDIS3 displays PIN domain-dependent endonucleolytic activity

To assess the biochemical activities of hDIS3 and hDIS3L, we first attempted their production in *E. coli* as either full-length or N- or C-terminal truncated variants (Supplementary Figure S6A). All designed versions of hDIS3 were obtained, but for hDIS3L only the C-terminal part corresponding to the RNase II/R homology region (hDIS3L Cterm) was soluble (Supplementary Figure S6B). Biochemical experiments using a 5′-radiolabelled oligoribonucleotide substrate composed of a 17 nt-long single strand followed by a 14-adenosine long tail (ss17-A_{14}) provided evidence for hDIS3 nucleolytic activity sensitive to the D487N mutation of a key residue in the C-terminal RNB domain (Supplementary Figure S6C and D). Disappointingly, however, the hDIS3L Cterm protein did not display any detectable nuclease activity. Moreover, we failed to detect endonuclease activity of the hDIS3 PIN domain (data not shown).

Instead, we turned to purification of hDIS3 and hDIS3L from HEK293 Flp-In T-REx cell lines that produce the following full-length variants of hDIS3 and hDIS3L: WT, RNB MUT (D487N and D486N, respectively) and DM (D146N, D487 and D62N, D486N, respectively) (Supplementary Figure S6A). These proteins were tagged at their C-terminus with

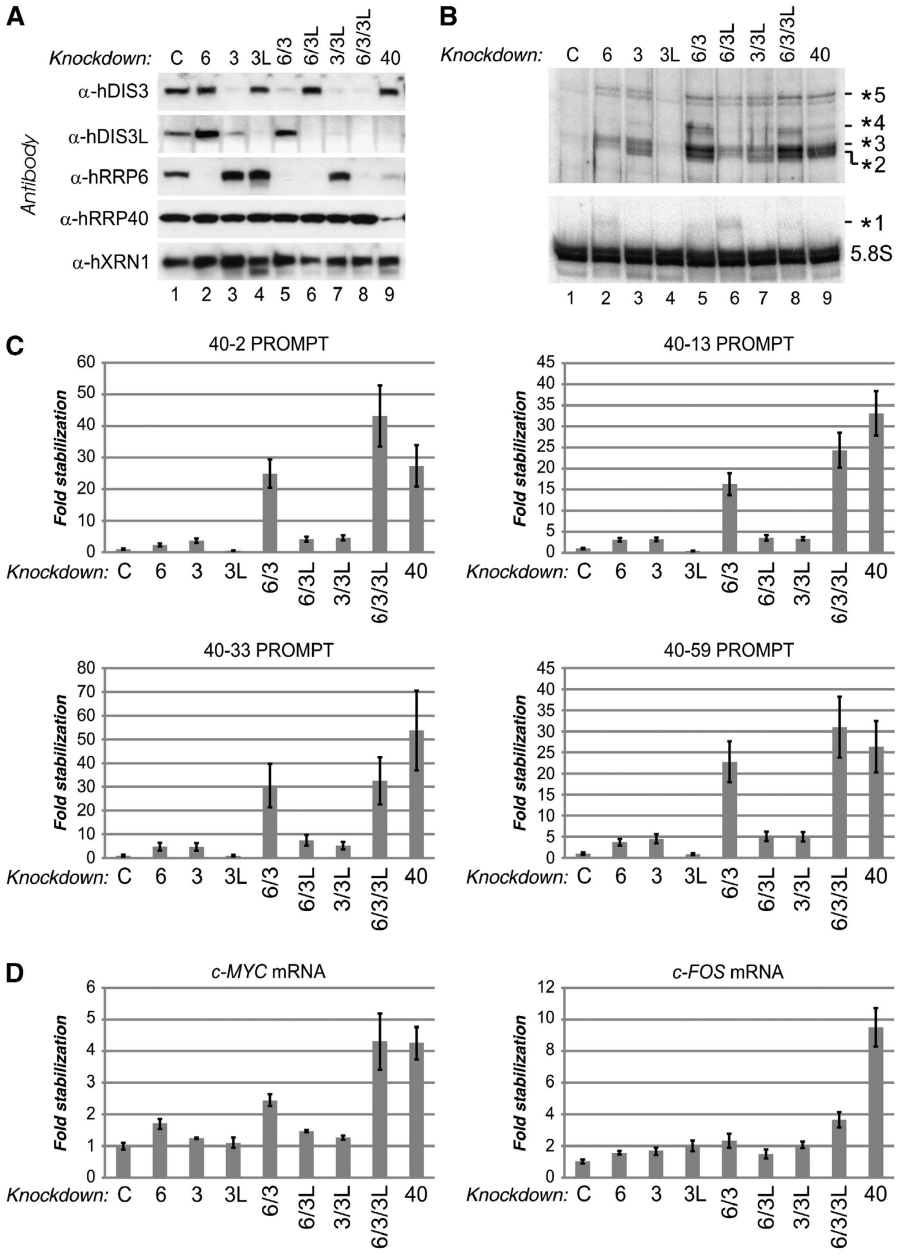

Figure 5 *In vivo* analyses of hDIS3, hDIS3L and hRRP6 substrate preferences. (**A**) Western blotting analysis of HeLa cells subjected to single, double or triple knockdown of hDIS3 (3), hDIS3L (3L) and hRRP6 (6) as well as single knockdown of hRRP40 (40) or treated with control siRNA, targeting eGFP (C). Anti-hDIS3, anti-hDIS3L, anti-hRRP6, anti-hRRP40 and anti-XRN1 (control) antibodies were used as indicated. (**B**) Northern blotting analysis of 5.8S rRNA and 3′end extended species present in total RNA samples harvested from cells (from (**A**)) subjected to the indicated factor depletions. The lower panel, corresponding to the lower part of the blot, shows mature 5.8S rRNA (4-min exposure) and the upper panel, corresponding to the upper part of the blot, shows 3′end extended variants (2-h exposure) each marked with an asterisk and a number. (**C**) RT–qPCR determination of levels of selected PROMPT (40-2, 40-13, 40-33 and 40-59) RNAs present in total RNA samples (from (**A**)). Histograms represent fold-change of the knockdown sample relative to the control (C) set to 1. All values were normalized internally to GAPDH RNA levels, which did not change significantly between the samples (s.d. are shown ($n=3$)). (**D**) RT–qPCR determination as in (**C**) of *c-MYC* and *c-FOS* RNA levels from the above-mentioned samples (**A**). Histograms and normalization are like in (**C**) (s.d. are shown ($n=3$)).

either FLAG or TAP epitopes and subsequently affinity purified using the appropriate resin. Relatively pure hDIS3-FLAG^{WT} and hDIS3-FLAG$^{RNB\ MUT}$ proteins were obtained (Supplementary Figure S7A) and biochemical assays performed using resin-immobilized protein demonstrated that hDIS3-FLAG^{WT} displays robust nucleolytic activity, whereas the hDIS3-FLAG$^{RNB\ MUT}$ control does not (Supplementary Figure S7B). This agrees with the results obtained from *E. coli* produced factors. Interestingly, we obtained very similar results for the analogous hDIS3L-FLAG^{WT} and hDIS3L-FLAG$^{RNB\ MUT}$ proteins (Supplementary Figure S7A and B), including an almost complete degradation of 5′-labelled ss17-A_{14} by the WT version. Thus, when isolated from human cells both hDIS3 and hDIS3L copurify with efficient nuclease activities.

To be able to use proteins, which were not resin immobilized, we turned to the TAP-tagged wild-type and mutant hDIS3 and hDIS3L constructs. In this case, we could not only

concentrate the fusion proteins on IgG-Sepharose resin (marked with open arrows in Figure 6A), but also cleave off the protein A tag, releasing the proteins into solution (Figure 6A; note the downshift of bands from lanes 'B' to 'EL'). Assayed as above, both hDIS3^{WT} and hDIS3L^{WT} exhibit nucleolytic activity on 5′-labelled ss17-A_{14}, whereas the hDIS3$^{RNB\ MUT}$ and hDIS3L$^{RNB\ MUT}$ variants do not (Figure 6B). Notably, the residual degradation observed for the RNB MUT versions is essentially the same as in the case of two negative controls (lanes 'empty vector' and 'no

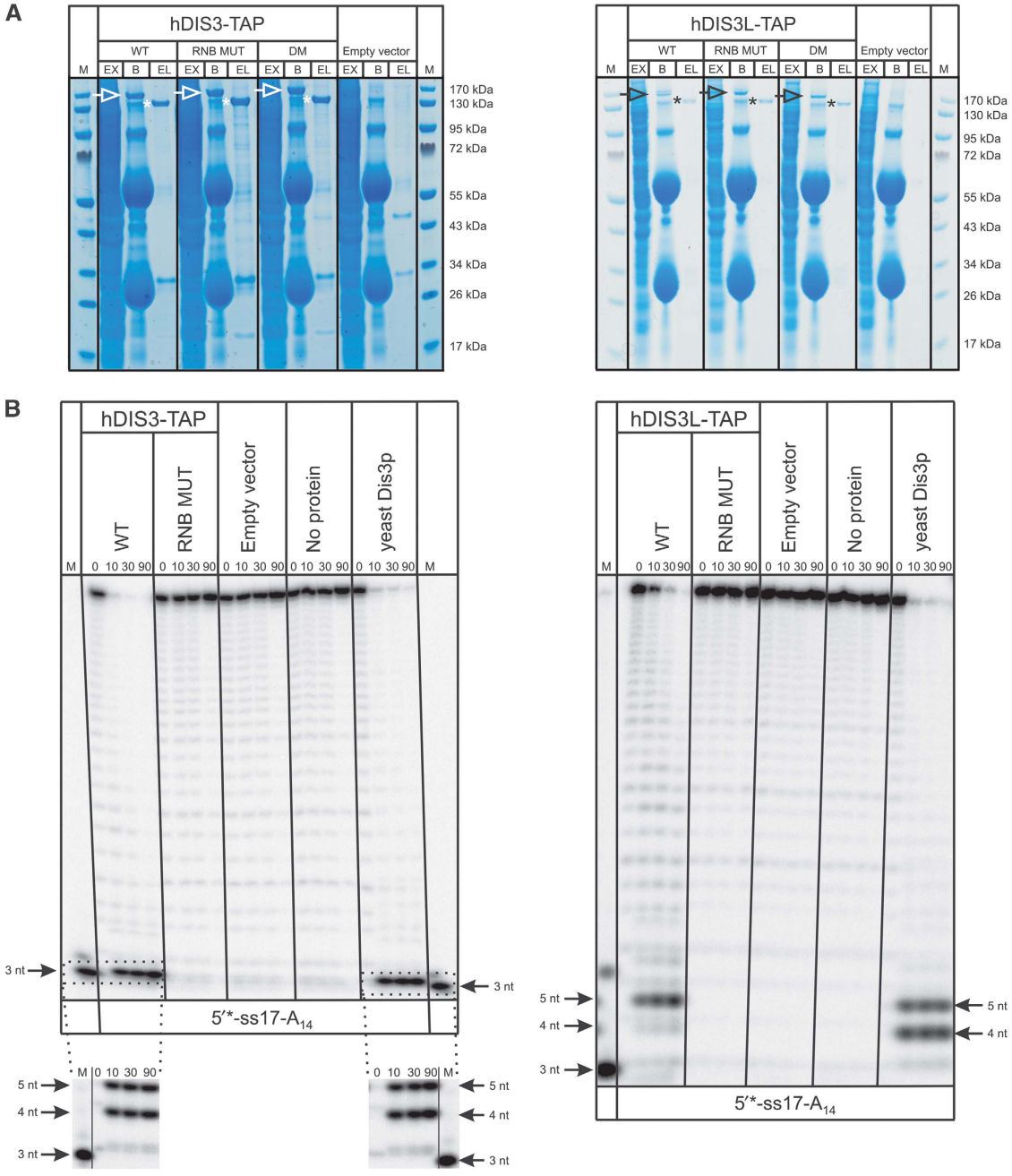

Figure 6 hDIS3 and hDIS3L are both 3′→5′ exoribonucleases. (**A**) NuPAGE analysis of TAP-tagged full-length hDIS3 (left panel) and hDIS3L (right panel) WT, RNB MUT and double RNB and PIN domain mutant (DM) variants affinity purified using the TAP protein A moiety. Positions of hDIS3/hDIS3L TAP fusions bound to IgG-Sepharose beads and cleaved/eluted proteins are marked with open arrows and asterisks, respectively. Parallel purification performed using cells transfected with an empty vector served as a negative control. Eluates were used in biochemical experiments shown in (**B**) and in Figure 7. Lane designations: EX—extract; B—IgG-resin with bound proteins; EL—elution by TEV protease cleavage; M—PageRuler Prestained Protein Ladder (Fermentas) with molecular masses indicated. (**B**) hDIS3 and hDIS3L display 3′→5′ exoribonuclease activity abolished by mutation of the RNB domain. 5′-labelled ss17-A_{14} substrate was incubated in a buffer containing 100 μM magnesium with hDIS3^{WT} (left panel) or hDIS3L^{WT} (right panel), their RNB MUT counterparts, an 'empty vector' control from (**A**) or in the absence of added protein. Full-length WT yeast Dis3p was used as a positive control. Reactions were terminated at the indicated time points followed by denaturing PAGE and phosphorimaging. Positions of 3 nt-long marker and 4–5 nt-long final degradation products, which were highly similar between *S. cerevisiae* Dis3p and hDIS3/hDIS3L proteins, are marked. In the case of hDIS3 (left panel), the reaction mixtures were re-run longer to better visualize the size of terminal degradation products (bottom). Final hDIS3, hDIS3L and Dis3p protein concentrations were 0.25, 0.04 and 0.2 μM, respectively.

protein'). The 4–5 nt lengths of the major end products generated by WT hDIS3 and hDIS3L is very similar to those produced by the documented processive 3′→5′ exoribonuclease activity of yeast Dis3p (Figure 6B; see also Lorentzen *et al*, 2008b). As the degradation patterns of 3′-labelled ss17-A_{14} (ss17-A_{14}-3′*) for yeast Dis3p and both human DIS3 proteins also resembled each other, including the predominance of a 3′-terminal mononucleotide as the major degradation product (Supplementary Figure S8), these data strongly suggest that RNB domains of hDIS3 and hDIS3L are associated with processive exonucleolytic activity working in the 3′→5′ direction, as for the yeast Dis3p catalytic exosome subunit.

As judged by PIN domain alignments, only hDIS3 is predicted to harbour endonucleolytic activity (Figure 1C). To test this prediction, RNB MUT and DM variants of hDIS3 were subjected to biochemical assays with differentially labelled ss17-A_{14} substrate. Reactions were carried out in a high manganese concentration buffer, which was optimal for revealing the endonucleolytic activity of the Dis3p PIN domain (Lebreton *et al*, 2008; Schaeffer *et al*, 2009; Schneider *et al*, 2009). Under these conditions, hDIS3$^{RNB\,MUT}$ was capable of degrading both 5′- and 3′-labelled ss17-A_{14}, producing a similar ladder of degradation products irrespective of the position of the radiolabel (Figure 7A). Furthermore, hDIS3$^{RNB\,MUT}$ was able to degrade circularized ss17-A_{14}, demonstrating that the degradation was endonucleolytic. This activity was detected not only with ss17-A_{14}, but also with two other 5′-labelled substrates: a related 17-mer with a 30-adenosine long tail (ss17-A_{30}) and a generic 44-mer devoid of an A-tail (ss44) (Supplementary Figure S9). Degradation of the ss17-A_{14} and ss17-A_{30} substrates was more efficient, indicating a preference for adenosine residues, as also observed for the Dis3p PIN domain (Lebreton *et al*, 2008). Notably, none of the tested substrates were degraded by the hDIS3^{DM} double mutant (Figure 7A; Supplementary Figure S9), strongly suggesting that the PIN domain is indeed responsible for the observed endonuclease activity. Conversely, neither hDIS3L$^{RNB\,MUT}$ nor hDIS3L^{DM} were able to degrade the linear 5′-labelled ss17-A_{30} or circular ss17-A_{14} substrates (Figure 7B). Notably, hDIS3$^{RNB\,MUT}$ at a concentration similar to hDIS3L proteins retained the ability to induce the decay of circularized ss17-A_{14} (Figure 7B). Moreover, lack of detectable hDIS3L$^{RNB\,MUT}$ nucleolytic activity was confirmed by changing the divalent cation type and/or concentration in the reaction mixture (Supplementary Figure S10).

We conclude that both hDIS3 and hDIS3L are processive 3′→5′ exonucleases owing to their RNB domains. In addition, hDIS3 is also endowed with endonucleolytic activity, which is strictly dependent on an intact PIN domain. On the other hand, and as predicted from the sequence, hDIS3L displays no endonucleolytic activity. Thus, hDIS3 is more similar to yeast Dis3p not only in terms of sequence conservation and intracellular localization, but also in the possession of two distinct ribonucleolytic activities residing in two independent domains. It is worth noting, however, that only the exonuclease activity of hDIS3 is essential for the complementation of a yeast Dis3p depletion (Supplementary Figure S11).

Discussion

Despite its presumed function as the primary 3′→5′ exonuclease in eukaryotes, major processive catalytic subunits of the human RNA exosome have escaped detection. So far the only identified interaction partner with enzymatic activity has been the distributive enzyme hRRP6. Here, we show that two human proteins homologous to the yeast essential catalytic subunit Dis3p—hDIS3 and hDIS3L—both physically interact with the catalytically inert nine-subunit core exosome. The identification of hDIS3L as a core exosome-associated factor has also been independently verified (Staals *et al*, 2010). We therefore propose that three ribonucleases, hDIS3, hDIS3L and hRRP6, serve as exosome catalytic subunits in humans, a scenario that likely holds for vertebrates in general, as predicted by phylogenetic analysis. The lack of earlier identification of hDIS3 and hDIS3L as human exosome subunits is most likely because of their lower affinity towards the exosome core relative to that of their yeast counterpart Dis3p; exosome components are only present in substoichiometric amounts when hDIS3 proteins are used as baits for affinity purifications. Hence, sensitive techniques, such as the SILAC-based methodology used here, are needed to reliably measure interactions above background. Although the salt-sensitive interaction of human DIS3 proteins with the exosome core may reflect a large unbound fraction of these proteins, we favor the alternative that irrespective of the seemingly weak interaction, hDIS3 and hDIS3L perform at least some of their cellular tasks as exosome subunits. This is because of our observation that the same strong stabilization phenotype of nuclear exosome substrates on depletion of the core component hRRP40 is only achieved by depleting both hDIS3 and hRRP6; their individual knockdowns do not yield the same robust effect (Figure 4B and C). This also indicates that functional redundancy exists between these catalytic subunits.

Unlike the suggested strict nuclear localization of yeast Rrp6p, its exact site of residence in human cells has been subject to some controversy. We have therefore conducted fluorescent microscopic analysis using several different reagents to visualize the intracellular localization of hDIS3, hDIS3L and hRRP6. These approaches largely agree with the results from an independent subcellular fractionation procedure and arrive at an unexpected conclusion: the three catalytic subunits display rather different localization patterns (Figure 8). In agreement with previously published results, hRRP6 is mainly nuclear with significant nucleolar enrichment (Allmang *et al*, 1999). Although the majority of hDIS3 is also nuclear, it is—in clear contrast to hRRP6—excluded from nucleoli. Finally, hDIS3L is a strictly cytoplasmic protein. Notably, in agreement with earlier reports (Lejeune *et al*, 2003; van Dijk *et al*, 2007) a minor pool of hRRP6 is also cytoplasmic. Interestingly, given the rough estimate of hRRP6 in ~10-fold molar excess to its processive enzyme counterparts, this observation may be of functional significance. Collectively, the data strongly suggest that several human exosome complexes exist with different combinations of catalytic subunits (Figure 8). Although an in-depth analysis of the functional implications of this observation is lacking, our results provide an insight into the specific substrate targeting reflected by this differential distribution of exonucleases on the human core exosome.

The situation in human cells therefore differs from yeast where only two forms of the exosome are thought to predominate: a cytoplasmic complex holding Dis3p and a nuclear complex harbouring both Dis3p and Rrp6p. We note that

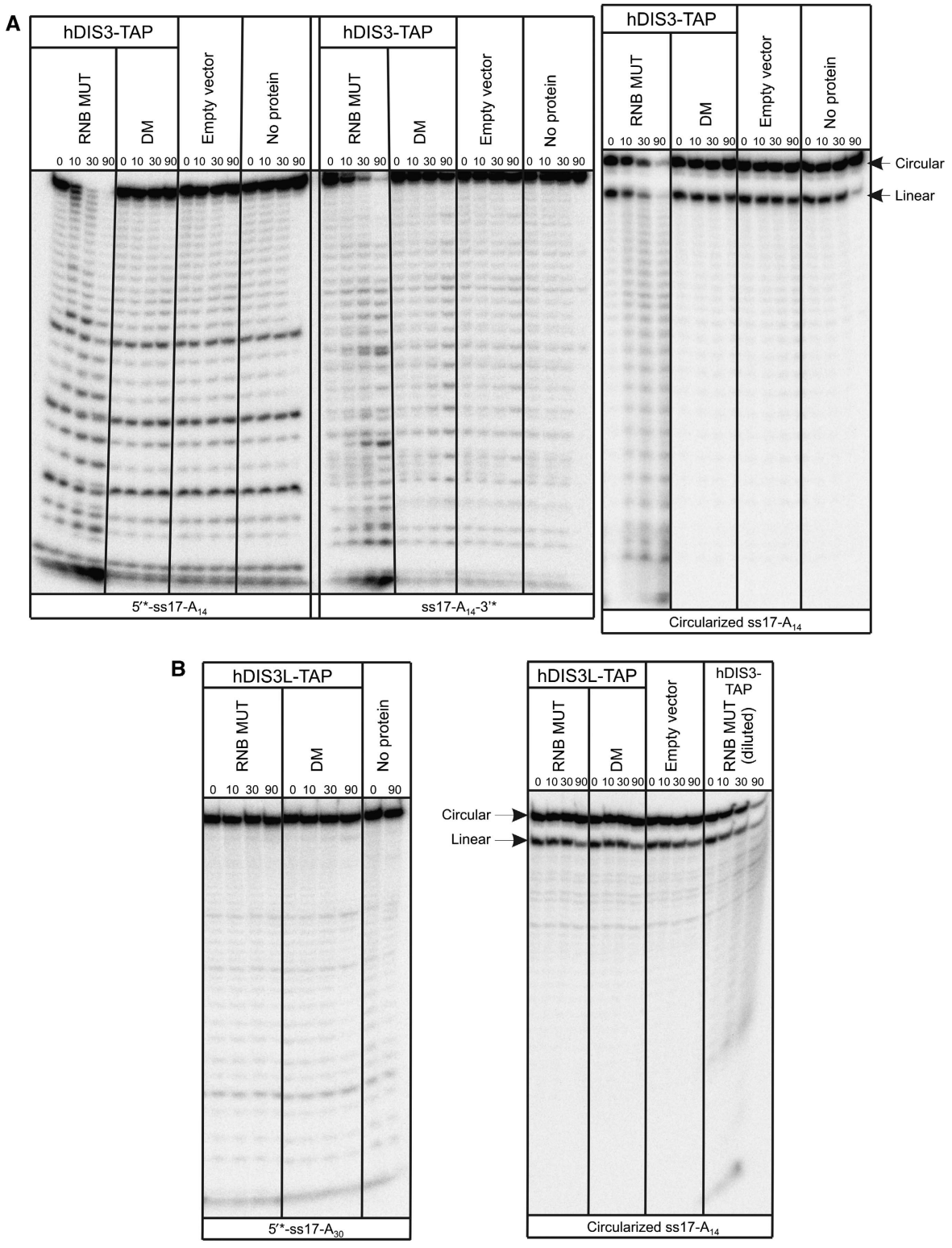

Figure 7 hDIS3, but not hDIS3L is endowed with PIN domain-dependent endoribonucleolytic activity. (**A**) hDIS3$^{RNB\,MUT}$ displays endonuclease activity, which is abolished by PIN domain mutation. 5′-labelled (left), 3′-labelled (middle) or circularized (right) ss17-A_{14} RNA substrates were incubated with hDIS3$^{RNB\,MUT}$, hDIS3^{DM}, an 'empty vector' control (all shown in Figure 6A) or in the absence of protein. The experiment was performed as in Figure 6B, only a buffer containing 3 mM manganese instead of 100 μM magnesium was used. The final hDIS3 protein concentration was 0.25 μM. (**B**) hDIS3L$^{RNB\,MUT}$ is catalytically inert. 5′-labelled ss17-A_{30} (left) or circularized ss17-A_{14} (right) substrates were incubated with hDIS3L$^{RNB\,MUT}$, hDIS3L^{DM} or in the absence of protein (shown in Figure 6A). Where indicated, an 'empty vector' control and hDIS3$^{RNB\,MUT}$ protein diluted to the same concentration as hDIS3L versions (0.04 μM) were also used. The experiment was performed as in (**A**).

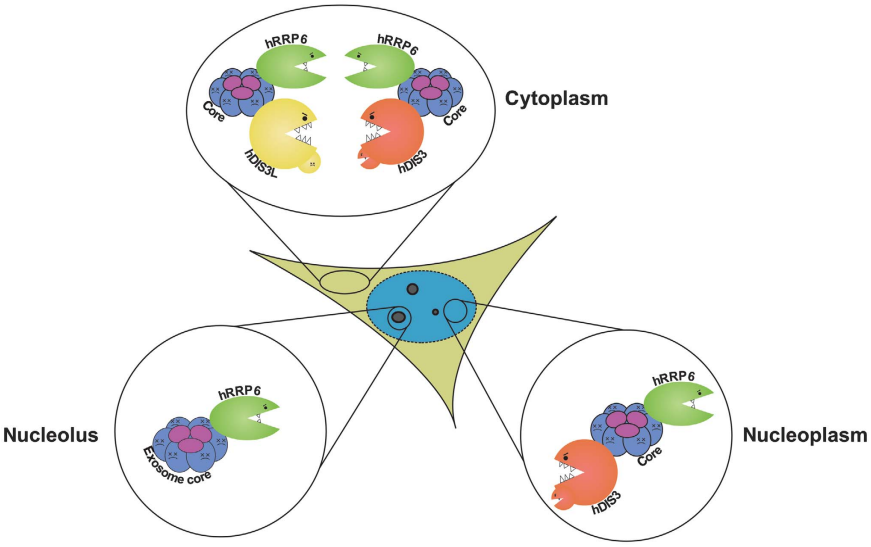

Figure 8 Differential compartmentalization of human exosome isoforms. Overview of the localization of catalytic exosome subunits. The ubiquitously present catalytically inert exosome core associates in the nucleus with the processive 3′→5′ exoRNase and endoRNase hDIS3, and with the distributive 3′→5′ exoRNase hRRP6. In the nucleolus, the core exosome primarily binds hRRP6. Finally, in the cytoplasm, the core associates with the cytoplasmic-restricted processive 3′→5′ exoRNase hDIS3L, which is devoid of endoRNase activity. Both hRRP6 and hDIS3 are also present in the cytoplasm, albeit in lower amounts than in the nucleus/nucleolus. It remains to be determined whether free core particles and catalytic subunits exist.

the interactions of hDIS3 and hDIS3L with the exosome core are most probably mutually exclusive. This is because their highly homologous PIN domains are predicted to be responsible for linking these factors to the core (Bonneau *et al*, 2009; Schneider *et al*, 2009). Consistently, we do not detect hDIS3 in hDIS3L pull downs and *vice versa*. Although both hDIS3 and hDIS3L, like their yeast counterpart, display processive exonuclease activity originating from their RNB domains, only the hDIS3 PIN domain harbours endonuclease activity. In yeast, this feature is believed to support the decay of structured RNA substrates, which predominate in the nucleus (Lebreton *et al*, 2008), it therefore appears reasonable that endonuclease activity has been retained in the one human Dis3p ortholog that resides in that compartment.

Exosome complexes from all eukaryotic kingdoms harbour a nine-subunit core structure. Only in plants has a core-associated phosphorolytic activity been preserved (Chekanova *et al*, 2000), whereas for all other eukaryotes examined so far, catalytic activity relies on the addition of hydrolytic cofactor ribonucleases, the number of which vary between different branches. Exosome-associated nucleases are either of the Dis3p- or Rrp6p-protein family, and for fungi, protists and invertebrates there is a single Dis3p and a single Rrp6p ortholog. In contrast, plants possess three different Rrp6p homologs (Lange *et al*, 2008) and vertebrates have two homologs of Dis3p. Further research will be aimed to uncover the functional significance of this assortment of different catalytic subunits of the exosome between organisms.

Materials and methods

In silico analyses

Homologs of *S. cerevisiae* Dis3p were searched by PSI-BLAST using the Dis3p amino-acid sequence as a query. Structure-assisted multiple sequence alignments were generated with PROMALS3D (Pei *et al*, 2008) using the crystal structure of Dis3p, PDB accession 2vnu (Lorentzen *et al*, 2008b) as reference, and subsequently manually edited using BioEdit (Hall, 1999). The maximum likelihood phylogenetic tree was calculated using the protml program of the Phylip package (Felsenstein, 1989), applying bootstrapping (1000 replicates) to ensure reliability. The tree image was created using Figtree (http://tree.bio.ed.ac.uk/software/figtree). The alignment image was generated using GeneDoc (Nicholas *et al*, 1997) and with the GNU Image Manipulation Program.

SILAC labelling and purification of proteins from human cells

Before coIP/MS analysis, two independent pools of the relevant HEK293 Flp-In T-REx cell line, harbouring a FLAG-tagged version of either hRRP41, hDIS3 or hDIS3L were grown in custom-synthesized DMEM SILAC media supplemented with 10% dialyzed foetal calf serum (Gibco), 100 U/ml penicillin, 100 μg/ml streptomycin and 2 mM L-glutamine for a minimum of five doublings (>7 days). Each pool was isotope labelled with Lys0/Arg0 or Lys4/Arg6 (Lys0: $^{12}C_6{}^{14}N_2$; Lys4: $^{2}H_4$ Arg0: $^{12}C_6{}^{14}N_4$ and Arg6: $^{13}C_6{}^{14}N_4$, Sigma-Isotec, St Louis, MO). At 24 h after seeding, fresh, preheated medium was added (Lys4/Arg6 medium containing 30 ng/ml tetracycline to test cells and Lys0/Arg0 medium without tetracycline to controls). After 24 h, cells were washed with phosphate-buffered saline (PBS) (13.7 mM NaCl; 0.27 mM KCl; 0.14 mM KH_2PO_4; 0.43 mM Na_2HPO_4), and scraped into RSB100 buffer (10 mM Tris–HCl, pH 7.4; 100 mM NaCl and 2.5 mM $MgCl_2$) containing 0.5% Triton X-100 and protease inhibitor (one Complete, mini, EDTA-free, Protease Inhibitor cocktail (Roche) tablet per 10 ml of buffer). Cell slurries were then sonicated on ice using a Branson Sonifier 250 at setting 1 (output: ~20 W) for 3 × 10 s, and subsequently centrifuged at 4000 *g* for 15 min at 4°C. Supernatants were treated with RNase A at a concentration of 100 μg/ml for 2 min and subjected to a final centrifugation step at 16 200 *g* for 1 min. Equal amounts of supernatants (cell extract) were loaded onto Agarose anti-FLAG (M2) beads (Sigma) pre-washed in RSB100 buffer, containing 0.5% Triton X-100 and incubated for 2 h at 4°C with constant movement. The two separate test and control volumes of resin were washed four times with RSB100, containing 0.5% Triton X-100 and then combined into one tube, followed by four washes in RSB100 and one wash in TBS (10 mM Tris–HCl, pH 7.4; 150 mM NaCl). The final washing steps ensured MS compatibility. Proteins from the mixed samples were eluted either overnight by incubation with 0.5 mg/ml FLAG peptide in TBS, or by a 5-min incubation with 2 × SDS

sample buffer (125 mM Tris–HCl, pH 6.8; 20% glycerol; 4% SDS; 0.01% bromophenol blue).

Sample preparation for MS analysis

Proteins were either digested in solution (for FLAG peptide-eluted samples), or separated by SDS–PAGE and digested in-gel with trypsin (for SDS-eluted samples). For in-solution digestion, proteins were denaturated with 8 M urea, and treated with LysC endopeptidase for 3 h at room temperature. The samples were then treated with ammoniumbicarbonate and trypsin overnight at 37°C. The next day, samples were treated with 10 mM dithiothreitol (DTT) for 20–30 min at 56°C, and alkylated with 55 mM iodoacetamide for 20 min in the dark. The resulting peptides were extracted with 1% trifluoroacetic acid and then concentrated and desalted using small reverse-phase C_{18} columns pre-washed with methanol, solution B (80% acetonitrile, 0.5% trifluoroacetic acid) and solution A (0.5% acetic acid). The peptides were washed twice with solution A and then eluted with buffer B into 96-well plates. The samples were dried and resuspended in 8 μl 2% trifluoroacetic acid for MS analysis.

MS and data analysis

MS analysis was performed by LC-MS using an Agilent HP1100 system and an LTQ-Orbitrap mass spectrometer (Thermo Fisher). Peptides were separated by a 120-min linear gradient of 95% solution A to 50% solution B (see above). The mass spectrometer was operated in the data-dependent mode to acquire high-resolution precursor ion spectra (m/z 300–1500, resolution 60 000 and ion accumulation to a target value of 5×10^6 ions) in the Orbitrap. The five most intense ions were sequentially isolated for accurate mass measurements and fragmentation in the linear ion trap.

Peak lists were extracted from the mass spectra using the program DTA supercharge or MaxQuant (Cox and Mann, 2008) and submitted for protein database searches (Human IPI version 3.52) using the Mascot program (Matrix Science). MaxQuant and MSQuant (an in-house developed open-source application, http://msquant.sourceforge.net/) were used to calculate peptide isotope ratios and to evaluate the certainty in peptide identification and quantitation based on Mascot score, false-discovery rates, or manual inspection. Proteins included in Supplementary Tables S1–S3 were identified by a false-discovery rate of 0.01 derived by decoy database searching. As an arbitrary cutoff ratio for specific versus nonspecific protein binders, the average s.d. of all the proteins identified in an experiment was multiplied by two, and added to 1. Thus, proteins with an SILAC ratio above $1 + 2x$ average s.d. (for all proteins identified in an experiment) are assumed to be true interaction partners.

Immunolocalization analysis

In general, cells were fixed with 3.7% formaldehyde in PBS for 15 min, permeabilized with 1% Triton X-100/10% FBS solution in PBS for 5 min and blocked for 1 h with 10% FBS solution in PBS (blocking solution). Cells were incubated in blocking solution, first with primary antibody for 1 h and then with secondary antibody for 1 h in the dark. Finally, cells were stained with Hoechst 33342 (Invitrogen) by incubation in a 10 μg/ml solution in PBS for 1 min and washed. All procedures were performed at 25°C, and cells were washed three times with PBS between each step. After the final wash, coverslips were mounted on slides in ProLong Gold antifade reagent (Invitrogen), left in the dark overnight at 25°C and then stored at 4°C until microscopic analysis.

For localization of endogenous proteins, HeLa and HEK293 Flp-In T-REx cells were plated on coverslips (coated with poly-D-lysine (Sigma-Aldrich) for HEK293 Flp-In T-REx cells) and 24 h later fixed and stained as above. For localization of myc-tagged hDIS3L, HEK293 Flp-In T-REx were transfected with Lipofectamine 2000 using pHEX17 construct. Twelve hours after transfection, cells were trypsinized and replated onto poly-D-lysine-coated coverslips placed in 60-mm culture dishes. On replating, the medium was supplemented with 100 ng/ml doxycycline (Sigma-Aldrich) to induce protein expression. In all cases cells were fixed, stained 24 h after transfection and imaged with an epifluorescent or a confocal microscope. Localization of FLAG-tagged proteins was performed in a similar way, using the appropriate stable HEK293 Flp-In T-REx cell lines.

The following antibodies were used (dilutions in parentheses): mouse monoclonal anti-myc, Santa Cruz Biotechnology (1:200); mouse monoclonal anti-FLAG (M2), Sigma-Aldrich (1:200); rabbit polyclonal anti-hRRP6, Sigma-Aldrich (1:200); Alexa Fluor 488-conjugated goat anti-rabbit IgG, Invitrogen (1:800); Alexa Fluor 488-conjugated donkey anti-rabbit IgG, Invitrogen (1:2000); Alexa Fluor 488-conjugated donkey anti-mouse IgG, Invitrogen (1:2000); Alexa Fluor 555-conjugated goat anti-mouse IgG, Molecular Probes (1:800); mouse polyclonal anti-hDIS3, Abnova (1:100–1:200), mouse polyclonal anti-hDIS3L, Abnova (1:100); rabbit polyclonal anti-hRRP40 (1:200) (kindly provided by Dr Ger Pruijn). Cells were imaged with an LSM 510 confocal microscope (Zeiss) using 405, 488 and 543 nm beams for excitation with proper emission filters for Hoechst 33342, Alexafluor 488 and Alexa Fluor 555, respectively. HEK293 Flp-In T-REx cell lines stained for FLAG-tagged and endogenous exosome components were visualized using an Axiovert 200 M (Zeiss) epifluorescent microscope equipped with a coolSNAP$_{HQ}$ camera (Photometrics).

Subcellular fractionation

The subcellular fractionation protocol used parts of published methods (Wuarin and Schibler, 1994; Mili and Pinol-Roma, 2003). In brief, 2.5×10^6 HEK293 Flp-In T-REx cells were plated onto a 100-mm plate and allowed to grow for 48 h. Cells were washed with PBS followed by a short incubation with trypsin/EDTA (Invitrogen) at room temperature. Cells were collected and detached from each other by gentle pipetting and centrifuged at 240 *g* at 4°C for 4 min. Subsequently, the cells were washed with ice-cold DMEM/10% FBS to inactivate trypsin and twice with ice-cold PBS. Washed cells were collected by centrifugation at 240 *g* for 1 min and resuspended in ice-cold hypotonic RSB-10 (10 mM Tris–HCl, pH 7.4; 10 mM NaCl; 2.5 mM $MgCl_2$) and allowed to swell by incubation on ice for 5 min. Next, a Dounce homogenizer (25 strokes) was used to break open cells and release nuclei, which were collected by centrifugation at 240 *g* for 5 min at 4°C. The supernatant was cleared by centrifugation at 20 000 *g* for 10 min at 4°C and kept as the cytoplasmic fraction (*cyt*). The nuclei were resuspended in S1 solution (0.25 M sucrose; 10 mM $MgCl_2$) and layered on top of an equal volume of S3 solution (0.88 M sucrose; 0.5 mM $MgCl_2$) followed by centrifugation at 2800 *g* for 10 min at 4°C. Pelleted nuclei were resuspended in ice-cold RSB-300U (10 mM Tris–HCl, pH 7.4; 2.5 mM $MgCl_2$; 300 mM NaCl; 1 M urea) supplemented with 0.5% Triton X-100, followed by vigorous agitation for about 15 s and incubated on ice for 10 min. Chromatin was collected by centrifugation at 15 000 *g* for 5 min and the supernatant was kept as the nucleoplasmic fraction (*nuc*). The chromatin pellet was resuspended in RSB-300U/0.5% Triton X-100 and sonicated at 4°C in a BioRuptor sonicator (Diagenode) using 2×9 pulses of 30 s at setting H (interrupted by 30 s pauses). The sonicated samples were centrifuged at 20 000 *g* for 10 min and the supernatant was kept as the chromatin fraction (*chr*).

Western blotting

Subcellular fractions and protein samples from coIP experiments were analysed by standard western-blot procedures (Sambrook and Russell, 2001) using the following antibodies: mouse monoclonal anti-FLAG (M2) (Sigma-Aldrich), rabbit polyclonal anti-UAP56 (kind gift from Dr Michael R Green), rabbit polyclonal anti-hRRP6 (Sigma-Aldrich), mouse polyclonal anti-hDIS3 (Abnova), mouse polyclonal anti-hDIS3L (Abnova), rabbit polyclonal anti-hRRP40 (kindly provided by Dr Ger Pruijn), rabbit polyclonal anti-hXRN1 (kind gift from Dr Jens Lykke-Andersen), rabbit polyclonal anti-tubulin (Rockland), rabbit polyclonal anti-histone H3 (Abcam) and mouse monoclonal anti-U1 70K (kindly provided by Dr Douglas Black).

Purification of proteins from human cells for biochemical analyses

Stable HEK293 Flp-In T-REx cell lines overexpressing different versions of FLAG- or TAP-tagged hDIS3 and hDIS3L were grown in 10 145 mm dishes. Induced cells were harvested in PBS at about 100% confluence, pelleted, frozen in liquid nitrogen and stored at −80°C. Cells were then resuspended in 5 ml of lysis buffer (20 mM Tris–HCl, pH 7.4; 75 mM NaCl for hDIS3 or 150 mM NaCl for hDIS3L; 1 mM DTT; 1% Triton X-100; 1 mM PMSF; 1× protease inhibitors cocktail: 0.02 μM pepstatinA, 0.02 μg/ml chymostatin, 0.006 μM leupeptin, 20 μM benzamidine hydrochloride) and incubated with rotation at 4°C for 30 min. Cells were then sonicated for 20 min (30 s pulses with 30 s intervals), after which the lysate

was cleared by centrifugation at 32 000 rpm for 15 min in a Beckman 35 Ti rotor.

For purification of FLAG-tagged hDIS3 and hDIS3L proteins, 600 μl of anti-FLAG M2 beads (Sigma-Aldrich), rinsed with the low-salt buffer (20 mM Tris–HCl, pH 7.4; 1 mM DTT; 1 mM PMSF; 1 × protease inhibitors cocktail; 75 mM NaCl or 150 mM NaCl for hDIS3 or hDIS3L, respectively) was incubated with extract for 3 h at 4°C with rotation. Resins were transferred to PolyPrep columns (Bio-Rad), washed extensively with low-salt buffer, followed by high-salt buffer (20 mM Tris–HCl, pH 7.4; 1 mM DTT; 1 mM PMSF; 1 × protease inhibitors cocktail; 500 mM NaCl or 1 M NaCl for hDIS3 or hDIS3L, respectively) and again with the low-salt buffer.

For purification of TAP-tagged hDIS3 and hDIS3L proteins, cell extract was incubated with 500 μl of IgG-Sepharose beads (GE Healthcare), rinsed with lysis buffer, after which proteins were bound to the resin as described above. After transferring to PolyPrep columns, resins were washed with IPP buffer (10 mM Tris–HCl, pH 7.4; 1 mM DTT; 1% Triton X-100; 1 mM PMSF; 1 × protease inhibitors cocktail) supplemented with 75 mM NaCl (IPP75) or 150 mM NaCl (IPP150) for hDIS3 and hDIS3L, respectively, and then with IPP supplemented by 500 mM NaCl or 1 M NaCl for hDIS3 and hDIS3L, respectively, before another wash with IPP75 and IPP150, and a final wash with TEV buffer (10 mM Tris–HCl, pH 7.4; 75 mM NaCl for hDIS3 or 150 mM NaCl for hDIS3L; 1 mM DTT). After these steps, resin-bound proteins were eluted by incubation with TEV protease in TEV buffer overnight at 4°C. Protein purity was assessed by standard SDS–PAGE or NuPAGE (Invitrogen) gel electrophoresis. Protein amounts were estimated by densitometric analysis of NuPAGE gels stained with SimplyBlue SafeStain (Invitrogen) using serial dilutions of BSA as a standard.

Ribonuclease assays

In vitro enzymatic assays were performed in 20 μl reaction volumes containing 10 mM Tris–HCl, pH 8.0; 75 mM NaCl and 1 mM 2-mercaptoethanol, supplemented with either $MgCl_2$, $MnCl_2$ or $ZnCl_2$ at different concentration (within the range 40 μM–3 mM). Protein concentration varied from 0.04 to 0.25 μM, whereas substrate concentration was 0.2 μM. Reactions were performed at 37°C for the indicated times and terminated by adding 20 μl of formamide loading dye (90% formamide; 20 mM EDTA; 0.03% bromophenol blue; 0.03% xylene cyanol in 1 × TBE). Reaction products were resolved on denaturing 20% polyacrylamide, 8 M urea, 1 × TBE gels and visualized using a FUJI PhosphorImager. Details on preparation of radiolabelled substrates and purification of recombinant proteins from *E. coli* can be found in the Supplementary data.

Yeast complementation assays

p415 vector (Mumberg *et al*, 1995) derivatives bearing different versions of hDIS3 and hDIS3L (pHEX22–pHEX26, pHEX34–pHEX35) were transformed into the *S. cerevisiae* BSY1883 strain (*KanMX6:TetOFF-DIS3* in BMA64 background) (Lebreton *et al*, 2008). The pBS3269 plasmid (Lebreton *et al*, 2008), encoding WT yeast Dis3p, and empty p415 vector served as positive and negative controls, respectively. Transformed cultures were grown in synthetic complete medium without leucine (SC-leu) at 30°C overnight before spotting serial dilutions onto two plates SC-leu plates in the absence or presence of doxycycline (20 μg/ml) to repress chromosomal, WT *DIS3* gene expression. Cell growth was analysed after 60 h of incubation at 30°C.

Supplementary data

Supplementary data are available at *The EMBO Journal* Online (http://www.embojournal.org).

Acknowledgements

We thank Karina H Jürgensen and Dorthe C Riishøj for excellent technical assistance. Michal Minczuk and Justo Javier Escobar-Cubiella are acknowledged for their help at the initial stage of the research. Moreover, we are grateful to Michael Rosbash for critical reading of the manuscript. Ger Pruijn, Douglas Black, Jens Lykke-Andersen, Michael Green and Monika Hejnowicz are thanked for their kind gifts of plasmid and antibodies. Research in the AD laboratory was funded by a Polish Ministry of Science and Higher Education grant (N N301 250836) to RT, project operated within the Foundation for Polish Science Team Programme cofinanced by the EU European Regional Development Fund, Operational Program Innovative Economy 2007-2013 and an EMBO installation grant. AC was supported by a mini-grant from the Faculty of Biology, University of Warsaw (BW-179110). RJS is the recipient of the Stipend for Young Researchers from the Foundation for Polish Science. Research in the THJ laboratory was supported by the Danish National Research Foundation, the Danish Cancer Society and the Danish Council for Independent Research (Natural Sciences). Finally, the project was supported by the European Science Foundation (ESF) under the EUROCORES Programme RNA Quality (AD and THJ) and the European Commission's 7th Framework Programme (grant agreement HEALTH-F4-2008-201648/PROSPECTS to JSA).

Author contributions: AC performed DNA and protein sequence analysis and preliminary IP/MS analysis. RT, SL-A, AC, KD, AP and PPS generated DNA constructs. RT, SL-A and AC established stable cell lines. MSK performed western blotting analyses and coimmunoprecipitations and conducted proteomic analyses with KML and JSA. RT and KD performed yeast complementation assays. SL-A, MSK, AC and RJS performed localization and fractionation studies. SL-A performed RNAi of exosome components followed by northern blotting analysis and RT–qPCR. RT carried out all biochemical experiments. RT, SL-A, AD and THJ designed the research and supervised the experiments. RT, AC, AD and THJ wrote the paper.

Conflict of interest

The authors declare that they have no conflict of interest.

References

Allmang C, Petfalski E, Podtelejnikov A, Mann M, Tollervey D, Mitchell P (1999) The yeast exosome and human PM-Scl are related complexes of 3′ → 5′ exonucleases. *Genes Dev* **13:** 2148–2158

Anderson JS, Parker RP (1998) The 3′ to 5′ degradation of yeast mRNAs is a general mechanism for mRNA turnover that requires the SKI2 DEVH box protein and 3′ to 5′ exonucleases of the exosome complex. *EMBO J* **17:** 1497–1506

Araki Y, Takahashi S, Kobayashi T, Kajiho H, Hoshino S, Katada T (2001) Ski7p G protein interacts with the exosome and the Ski complex for 3′-to-5′ mRNA decay in yeast. *EMBO J* **20:** 4684–4693

Bonneau F, Basquin J, Ebert J, Lorentzen E, Conti E (2009) The yeast exosome functions as a macromolecular cage to channel RNA substrates for degradation. *Cell* **139:** 547–559

Bousquet-Antonelli C, Presutti C, Tollervey D (2000) Identification of a regulated pathway for nuclear pre-mRNA turnover. *Cell* **102:** 765–775

Camblong J, Iglesias N, Fickentscher C, Dieppois G, Stutz F (2007) Antisense RNA stabilization induces transcriptional gene silencing via histone deacetylation in *S.cerevisiae*. *Cell* **131:** 706–717

Chekanova JA, Shaw RJ, Wills MA, Belostotsky DA (2000) Poly(A) tail-dependent exonuclease AtRrp41p from *Arabidopsis thaliana* rescues 5.8 S rRNA processing and mRNA decay defects of the yeast ski6 mutant and is found in an exosome-sized complex in plant and yeast cells. *J Biol Chem* **275:** 33158–33166

Chen CY, Gherzi R, Ong SE, Chan EL, Raijmakers R, Pruijn GJ, Stoecklin G, Moroni C, Mann M, Karin M (2001) AU binding proteins recruit the exosome to degrade ARE-containing mRNAs. *Cell* **107:** 451–464

Cox J, Mann M (2008) MaxQuant enables high peptide identification rates, individualized p.p.b.-range mass accuracies and proteome-wide protein quantification. *Nat Biotechnol* **26:** 1367–1372

Doma MK, Parker R (2007) RNA quality control in eukaryotes. *Cell* **131:** 660–668

Dziembowski A, Lorentzen E, Conti E, Seraphin B (2007) A single subunit, Dis3, is essentially responsible for yeast exosome core activity. *Nat Struct Mol Biol* **14:** 15–22

Felsenstein J (1989) PHYLIP—Phylogeny Inference Package (Version 3.2). *Cladistics* **5:** 164–166

Frazao C, McVey CE, Amblar M, Barbas A, Vonrhein C, Arraiano CM, Carrondo MA (2006) Unravelling the dynamics of RNA degradation by ribonuclease II and its RNA-bound complex. *Nature* **443:** 110–114

Gherzi R, Lee KY, Briata P, Wegmuller D, Moroni C, Karin M, Chen CY (2004) A KH domain RNA binding protein, KSRP, promotes ARE-directed mRNA turnover by recruiting the degradation machinery. *Mol Cell* **14:** 571–583

Hall TA (1999) BioEdit: a user-friendly biological sequence alignment editor and analyses program for Windows 95/98/NT. *Nucleic Acids Symp Ser* **41:** 95–98

Hernandez H, Dziembowski A, Taverner T, Seraphin B, Robinson CV (2006) Subunit architecture of multimeric complexes isolated directly from cells. *EMBO Rep* **7:** 605–610

Hilleren P, McCarthy T, Rosbash M, Parker R, Jensen TH (2001) Quality control of mRNA 3′-end processing is linked to the nuclear exosome. *Nature* **413:** 538–542

Houseley J, LaCava J, Tollervey D (2006) RNA-quality control by the exosome. *Nat Rev Mol Cell Biol* **7:** 529–539

Houseley J, Rubbi L, Grunstein M, Tollervey D, Vogelauer M (2008) A ncRNA modulates histone modification and mRNA induction in the yeast GAL gene cluster. *Mol Cell* **32:** 685–695

Houseley J, Tollervey D (2009) The many pathways of RNA degradation. *Cell* **136:** 763–776

Isken O, Maquat LE (2007) Quality control of eukaryotic mRNA: safeguarding cells from abnormal mRNA function. *Genes Dev* **21:** 1833–1856

Kammler S, Lykke-Andersen S, Jensen TH (2008) The RNA exosome component hRrp6 is a target for the 5-fluorouracil in human cells. *Mol Cancer Res* **6:** 990–995

LaCava J, Houseley J, Saveanu C, Petfalski E, Thompson E, Jacquier A, Tollervey D (2005) RNA degradation by the exosome is promoted by a nuclear polyadenylation complex. *Cell* **121:** 713–724

Lange H, Holec S, Cognat V, Pieuchot L, Le Ret M, Canaday J, Gagliardi D (2008) Degradation of a polyadenylated rRNA maturation by-product involves one of the three RRP6-like proteins in *Arabidopsis thaliana*. *Mol Cell Biol* **28:** 3038–3044

Lebreton A, Seraphin B (2008) Exosome-mediated quality control: substrate recruitment and molecular activity. *Biochim Biophys Acta* **1779:** 558–565

Lebreton A, Tomecki R, Dziembowski A, Seraphin B (2008) Endonucleolytic RNA cleavage by a eukaryotic exosome. *Nature* **456:** 993–996

Lejeune F, Li X, Maquat LE (2003) Nonsense-mediated mRNA decay in mammalian cells involves decapping, deadenylating, and exonucleolytic activities. *Mol Cell* **12:** 675–687

Libri D, Dower K, Boulay J, Thomsen R, Rosbash M, Jensen TH (2002) Interactions between mRNA export commitment, 3′-end quality control, and nuclear degradation. *Mol Cell Biol* **22:** 8254–8266

Liu Q, Greimann JC, Lima CD (2006) Reconstitution, activities, and structure of the eukaryotic RNA exosome. *Cell* **127:** 1223–1237

Lorentzen E, Basquin J, Conti E (2008a) Structural organization of the RNA-degrading exosome. *Curr Opin Struct Biol* **18:** 709–713

Lorentzen E, Basquin J, Tomecki R, Dziembowski A, Conti E (2008b) Structure of the active subunit of the yeast exosome core, Rrp44: diverse modes of substrate recruitment in the RNase II nuclease family. *Mol Cell* **29:** 717–728

Lykke-Andersen S, Brodersen DE, Jensen TH (2009) Origins and activities of the eukaryotic exosome. *J Cell Sci* **122:** 1487–1494

Mili S, Pinol-Roma S (2003) LRP130, a pentatricopeptide motif protein with a noncanonical RNA-binding domain, is bound *in vivo* to mitochondrial and nuclear RNAs. *Mol Cell Biol* **23:** 4972–4982

Mitchell P, Petfalski E, Shevchenko A, Mann M, Tollervey D (1997) The exosome: a conserved eukaryotic RNA processing complex containing multiple 3′→5′ exoribonucleases. *Cell* **91:** 457–466

Mukherjee D, Gao M, O'Connor JP, Raijmakers R, Pruijn G, Lutz CS, Wilusz J (2002) The mammalian exosome mediates the efficient degradation of mRNAs that contain AU-rich elements. *EMBO J* **21:** 165–174

Mullen TE, Marzluff WF (2008) Degradation of histone mRNA requires oligouridylation followed by decapping and simultaneous degradation of the mRNA both 5′ to 3′ and 3′ to 5′. *Genes Dev* **22:** 50–65

Mumberg D, Muller R, Funk M (1995) Yeast vectors for the controlled expression of heterologous proteins in different genetic backgrounds. *Gene* **156:** 119–122

Neil H, Malabat C, d'Aubenton-Carafa Y, Xu Z, Steinmetz LM, Jacquier A (2009) Widespread bidirectional promoters are the major source of cryptic transcripts in yeast. *Nature* **457:** 1038–1042

Nicholas KB, Nicholas Jr HB, Deerfield II DW (1997) GeneDoc: analysis and visualization of genetic variation. *EMBNEW.NEWS* **4:** 14

Ong SE, Foster LJ, Mann M (2003) Mass spectrometric-based approaches in quantitative proteomics. *Methods* **29:** 124–130

Orban TI, Izaurralde E (2005) Decay of mRNAs targeted by RISC requires XRN1, the Ski complex, and the exosome. *RNA* **11:** 459–469

Pei J, Kim BH, Grishin NV (2008) PROMALS3D: a tool for multiple protein sequence and structure alignments. *Nucleic Acids Res* **36:** 2295–2300

Preker P, Nielsen J, Kammler S, Lykke-Andersen S, Christensen MS, Mapendano CK, Schierup MH, Jensen TH (2008) RNA exosome depletion reveals transcription upstream of active human promoters. *Science* **322:** 1851–1854

Rougemaille M, Gudipati RK, Olesen JR, Thomsen R, Seraphin B, Libri D, Jensen TH (2007) Dissecting mechanisms of nuclear mRNA surveillance in THO/sub2 complex mutants. *EMBO J* **26:** 2317–2326

Saguez C, Schmid M, Olesen JR, Ghazy MA, Qu X, Poulsen MB, Nasser T, Moore C, Jensen TH (2008) Nuclear mRNA surveillance in THO/sub2 mutants is triggered by inefficient polyadenylation. *Mol Cell* **31:** 91–103

Sambrook J, Russell DW (2001) *Molecular Cloning: A Laboratory Manual*. Cold Spring Harbor, NY, USA: Cold Spring Harbor Laboratory Press

Schaeffer D, Tsanova B, Barbas A, Reis FP, Dastidar EG, Sanchez-Rotunno M, Arraiano CM, van Hoof A (2009) The exosome contains domains with specific endoribonuclease, exoribonuclease and cytoplasmic mRNA decay activities. *Nat Struct Mol Biol* **16:** 56–62

Schilders G, Raijmakers R, Raats JM, Pruijn GJ (2005) MPP6 is an exosome-associated RNA-binding protein involved in 5.8S rRNA maturation. *Nucleic Acids Res* **33:** 6795–6804

Schilders G, van Dijk E, Pruijn GJ (2007) C1D and hMtr4p associate with the human exosome subunit PM/Scl-100 and are involved in pre-rRNA processing. *Nucleic Acids Res* **35:** 2564–2572

Schmid M, Jensen TH (2008a) The exosome: a multipurpose RNA-decay machine. *Trends Biochem Sci* **33:** 501–510

Schmid M, Jensen TH (2008b) Quality control of mRNP in the nucleus. *Chromosoma* **117:** 419–429

Schneider C, Leung E, Brown J, Tollervey D (2009) The N-terminal PIN domain of the exosome subunit Rrp44 harbors endonuclease activity and tethers Rrp44 to the yeast core exosome. *Nucleic Acids Res* **37:** 1127–1140

Shiomi T, Fukushima K, Suzuki N, Nakashima N, Noguchi E, Nishimoto T (1998) Human dis3p, which binds to either GTP- or GDP-Ran, complements *Saccharomyces cerevisiae dis3*. *J Biochem* **123:** 883–890

Slomovic S, Fremder E, Staals RH, Pruijn GJ, Schuster G (2010) Addition of poly(A) and poly(A)-rich tails during RNA degradation in the cytoplasm of human cells. *Proc Natl Acad Sci USA* **107:** 7404–7412

Staals RHJ, Bronkhorst AW, Schilders G, Slomovic S, Schuster G, Heck AJR, Raijmakers R, Pruijn GJM (2010) Dis3-like 1: a novel exoribonuclease associated with the human exosome. *EMBO J* **29:** 2358–2367

Torchet C, Bousquet-Antonelli C, Milligan L, Thompson E, Kufel J, Tollervey D (2002) Processing of 3′-extended read-through transcripts by the exosome can generate functional mRNAs. *Mol Cell* **9:** 1285–1296

van Dijk EL, Schilders G, Pruijn GJ (2007) Human cell growth requires a functional cytoplasmic exosome, which is involved in various mRNA decay pathways. *RNA* **13:** 1027–1035

Vanacova S, Stefl R (2007) The exosome and RNA quality control in the nucleus. *EMBO Rep* **8:** 651–657

Vasiljeva L, Buratowski S (2006) Nrd1 interacts with the nuclear exosome for 3′ processing of RNA polymerase II transcripts. *Mol Cell* **21:** 239–248

West S, Gromak N, Norbury CJ, Proudfoot NJ (2006) Adenylation and exosome-mediated degradation of cotranscriptionally cleaved pre-messenger RNA in human cells. *Mol Cell* **21:** 437–443

Wuarin J, Schibler U (1994) Physical isolation of nascent RNA chains transcribed by RNA polymerase II: evidence for cotranscriptional splicing. *Mol Cell Biol* **14:** 7219–7225

Wyers F, Rougemaille M, Badis G, Rousselle JC, Dufour ME, Boulay J, Regnault B, Devaux F, Namane A, Seraphin B, Libri D, Jacquier A (2005) Cryptic pol II transcripts are degraded by a nuclear quality control pathway involving a new poly(A) polymerase. *Cell* **121:** 725–737

Xu Z, Wei W, Gagneur J, Perocchi F, Clauder-Munster S, Camblong J, Guffanti E, Stutz F, Huber W, Steinmetz LM (2009) Bidirectional promoters generate pervasive transcription in yeast. *Nature* **457:** 1033–1037

Zuo Y, Vincent HA, Zhang J, Wang Y, Deutscher MP, Malhotra A (2006) Structural basis for processivity and single-strand specificity of RNase II. *Mol Cell* **24:** 149–156